



**HAL**  
open science

## A multi-temporal method for cloud detection, applied to FORMOSAT-2, VEN $\mu$ S, LANDSAT and SENTINEL-2 images

Olivier Hagolle, Mireille Huc, Villa Pascual David, Gérard Dedieu

### ► To cite this version:

Olivier Hagolle, Mireille Huc, Villa Pascual David, Gérard Dedieu. A multi-temporal method for cloud detection, applied to FORMOSAT-2, VEN $\mu$ S, LANDSAT and SENTINEL-2 images. Remote Sensing of Environment, 2010, 114 (8), pp.1747-1755. 10.1016/j.rse.2010.03.002 . hal-00489793

**HAL Id: hal-00489793**

**<https://hal.science/hal-00489793>**

Submitted on 29 Nov 2012

**HAL** is a multi-disciplinary open access archive for the deposit and dissemination of scientific research documents, whether they are published or not. The documents may come from teaching and research institutions in France or abroad, or from public or private research centers.

L'archive ouverte pluridisciplinaire **HAL**, est destinée au dépôt et à la diffusion de documents scientifiques de niveau recherche, publiés ou non, émanant des établissements d'enseignement et de recherche français ou étrangers, des laboratoires publics ou privés.

1 A multi-temporal method for cloud detection, applied to FORMOSAT-2,  
2 VEN $\mu$ S, LANDSAT and SENTINEL-2 images

3

4 O. Hagolle<sup>1,2</sup>, M. Huc<sup>2</sup>, D.Villa Pascual<sup>1</sup>, G. Dedieu<sup>2</sup>

5 1 CNES, 18 avenue Edouard Belin, 31401 TOULOUSE Cedex 4. Olivier.Hagolle@cnes.fr

6 2 CESBIO, Université de Toulouse, Unité mixte CNES CNRS IRD UPS, 18, avenue Edouard Belin, 31401  
7 Toulouse Cedex 4, France

8

9 ABSTRACT –

10 *Over lands, the cloud detection on remote sensing images is not an easy task, because of the*  
11 *frequent difficulty to distinguish clouds from the underlying landscape, even at a high resolution.*

12 *Up to now, most high resolution images have been distributed without an associated cloud mask.*

13 *This situation should change in the near future, thanks to two new satellite missions that will*  
14 *provide optical images combining 3 features : high spatial resolution, high revisit frequency and*  
15 *constant viewing angles. The VEN $\mu$ S (French and Israeli cooperation) mission should be launched*  
16 *in 2012 and the European SENTINEL-2 mission in 2013. Fortunately, two existing satellite*  
17 *missions, FORMOSAT-2 and LANDSAT, enable to simulate the future data of these sensors.*

18 *Multi-temporal imagery at constant viewing angles provides a new way to discriminate clouded*  
19 *and unclouded pixels, using the relative stability of the earth surface reflectances compared to the*  
20 *quick variations of the reflectance of pixels affected by clouds. In this study, we have used time*  
21 *series of images from FORMOSAT-2 and LANDSAT to develop and test a Multi-Temporal Cloud*  
22 *Detection (MTCD) method. This algorithm combines a detection of a sudden increase of reflectance*  
23 *in the blue wavelength on a pixel by pixel basis, and a test of the linear correlation of pixel*  
24 *neighborhoods taken from couples of images acquired successively.*

25 *MTCD cloud masks are compared with cloud cover assessments obtained from FORMOSAT2 and*  
26 *LANDSAT data catalogs. The results show that the MTCD method provides a better discrimination*  
27 *of clouded and unclouded pixels than usual methods based on thresholds applied to reflectances or*

28 *reflectance ratios. This method will be used within VEN $\mu$ S level 2 processing and will be proposed*  
29 *for SENTINEL-2 level 2 processing.*

## 30 **1. Introduction**

31 Cloud detection is one of the first difficulties encountered when trying to automatically process  
32 optical remote sensing data ; for instance, atmospheric correction, land cover classifications, change  
33 detection or inversion of biophysical variables require a preliminary step of cloud detection. Cloud  
34 detection is easier above water, because water has a uniform and low reflectance in the near infrared  
35 (except in sun glint geometry), but is much more difficult over land : even at high resolution, when  
36 clouds are much larger than pixel size, it is not easy to tell some thin clouds apart from the  
37 underlying landscape.

38 Most of the currently operational cloud screening methods were developed for moderate resolution  
39 sensors. The algorithms are highly dependent on the available spectral bands, many of them work  
40 on pixel by pixel basis (Bréon and Colzy, 1999, Lissens et al, 2000), some use neighborhood  
41 information, such as local standard deviation (Saunders and Kriebel, 1988, Ackerman et al, 1998).  
42 When available, thermal infrared bands are used to detect clouds colder than the earth surface,  
43 which corresponds to almost all types of clouds except thin or low clouds (Saunders and Kriebel,  
44 1988, Ackerman et al 1998). Thresholds on reflectance in the blue are better suited to detect low  
45 clouds, but they may fail when the earth surface is bright (Bréon and Colzy, 1999). Short Wave  
46 Infra Red (SWIR) bands are often used to tell snow apart from clouds : these targets have similar  
47 reflectance ranges in the visible and near infrared, but the SWIR reflectance of snow is much lower  
48 than that of clouds (Dozier, 1989). Among the SWIR bands, the 1380 nm band is located in a very  
49 strong water vapor absorption band, such that only the upper layers of the atmosphere are visible  
50 and the background is completely black. This band has been successfully used for MODIS project  
51 to detect high clouds (Gao et al, 1993), and the method works well even with thin cirrus clouds  
52 which are very difficult to detect otherwise (Lavanant, 2007).

53 Only a few algorithms use multi temporal observations to detect clouds : some of them compare the

54 processed product to a multi year monthly average of surface reflectance (Ackerman et al, 1998,  
55 Bréon and Colzy, 1999) ; Lyapustin et al 2008 relied on the hypothesis that the presence of a cloud  
56 is likely if a low correlation is observed at local scale between two successive images of the same  
57 zone; Reuter and Fisher, 2004, used the smooth variations of land surface temperatures observed  
58 within a day, to classify outliers as clouds on Meteosat Geostationary satellite images.

59 Until recently, given the cost of high resolution images, most users only ordered images with a very  
60 low cloud cover, and moreover, very few users have had access to time series with more than 10  
61 images. For such a small number of images, it is possible to discard the clouds manually (see for  
62 instance Wilson and Sader, 2002). Consequently, very few studies focused on the automatic cloud  
63 detection at high resolution (Wang et Ono, 1999). Space agencies and image distributors have  
64 developed algorithms to deliver a cloud notation within their image catalogs (Irish, 2000, Irish et al,  
65 2006, Latry et al, 2007), but their aim is only to help the user to choose the images to order : no  
66 cloud mask is provided with LANDSAT and SPOT products.

67 In 2009, the LANDSAT archive images became freely available, and in the near future, time series  
68 of VEN $\mu$ S (Dedieu et al 2006) and SENTINEL-2 (Martimor et al 2007) images will also be freely  
69 delivered to research users at least. As a result, time series of 50 to 100 images will become  
70 common, and an automatic cloud detection will be requested both by users and for the production of  
71 higher level products.

72 One important and original characteristic of VEN $\mu$ S and SENTINEL-2 images is that a given site  
73 will be acquired with constant observation angles at a constant local hour, and thus the directional  
74 effects (Roujean et al, 1992, Maignan et al, 2004) will be minimized. And thanks to the use of a  
75 sun-synchronous orbit, the variation of sun angles is also quite slow (near the equinoxes at 45°  
76 latitude, it can reach 10 degrees in a month). The surface reflectance variations above land due to  
77 sun angle variations within a month are usually below 5%, except near the backscattering direction  
78 (5 to 10 degrees distance). Backscattering observations are not possible for LANDSAT, they were  
79 avoided for our FORMOSAT time series and they will be avoided with VEN $\mu$ S. The surface  
80 reflectance of a land pixel usually varies very slowly with time, especially at short wavelengths

81 (400-500nm). As a result, a significant increase of reflectance in this wavelength range is very  
82 likely to be due to the appearance of a cloud. This criterion should provide a better discrimination  
83 than the classical approaches based on a threshold on reflectance in the blue spectral bands.

84 The Multi Temporal Cloud Detection (MTCD) method presented hereafter will be included in  
85 VEN $\mu$ S operational level 2 processing, as a preliminary step of the atmospheric correction. The  
86 atmospheric correction also is based on a multi-temporal method (Hagolle et al, 2008) and requires  
87 a very strict cloud mask. The MTCD mask will also be used to compute level 3 products (cloud free  
88 time composites) and it will be distributed to the users with each level 2 product. A cloud shadow  
89 detection has also been developed, based on the geometrical projection of the clouds detected,  
90 similarly to the work of Le Hegarat-Mascle, 2009, but describing this algorithm is out of the scope  
91 of the paper.

92 The next chapters detail successively the data sets, the cloud detection method, and the results we  
93 obtained.

94

## 95 **2.Data Sets used in the study**

96 Table 1 summarizes the characteristics of the sensors used for this study. VEN $\mu$ S (Dedieu et al,  
97 2006) is a scientific micro-satellite that results from a cooperation between the Israeli Space Agency  
98 (ISA) and the French Centre National d'Etudes Spatiales (CNES). VEN $\mu$ S will be launched no  
99 sooner than 2012. Its aim is to demonstrate the usefulness of repetitive acquisitions of high  
100 resolution images to monitor the dynamics of land surfaces, and especially vegetation. At least fifty  
101 sites around the world will be imaged by VEN $\mu$ S, every second day, during two years. The  
102 resolution of VEN $\mu$ S products will be 10m, with a field of view of 27km. Thanks to the orbital  
103 repeat cycle of 2 days, a given site will be observed with a constant viewing angle. The instrument  
104 will deliver images in 12 narrow spectral bands ranging from 415 nm to 910 nm.

105 The SENTINEL-2 satellites (Martimor et al, 2007) will generalize VEN $\mu$ S measurements to the  
106 whole land surfaces : it is an operational mission from the European Space Agency (ESA), based  
107 on two satellites scheduled to be launched respectively in 2013 and 2014. SENTINEL-2 will  
108 acquire high resolution images (10 to 60 m depending on the spectral band), with a field of view of  
109 300 km. The orbital repeat cycle is 10 days and 2 satellites will be placed on that orbit with a 180°  
110 angular distance: the two satellites will achieve a 5 days revisit period. As all the images will be  
111 acquired at Nadir, a given point on the earth will be observed at a constant viewing angle. The  
112 thirteen spectral bands of SENTINEL-2 range from visible to SWIR and are listed in table 1.

113 FORMOSAT-2 is a Taiwanese Satellite that provides data very similar to VEN $\mu$ S. It is possible to  
114 obtain 8m resolution images, every day, with constant viewing angles since FORMOSAT-2 orbit  
115 has a one day repeat cycle. The field of view is 24 km, and 4 spectral bands (490, 560, 660 and 820  
116 nm) are available. Up to now, given the cost of each image, few users have ordered such time series  
117 yet.

118 In the framework of VEN $\mu$ S preparation, CNES has purchased about 10 such time series, with a  
119 tentative acquisition every 5 days on average, and observation durations from 2 months to 4 years.  
120 These time series correspond to very different sites such as agricultural sites in temperate regions, a

121 conifer forest, agricultural sites in semi arid regions, mountains with snow , and a Sahelian site. For  
122 two of these sites (Muret, South west France, and Tensift, Morocco), in 2006, we ordered for a  
123 systematic acquisition and production of images, cloudy or not, while for the other sites and the  
124 other years, for cost reasons, only images with low cloud coverage were purchased. For this reason,  
125 only Muret and Tensift time series are fully suited to validate the cloud cover estimates in cloudy,  
126 clear and mixed cases (See table 2 for site coordinates). FORMOSAT-2 images were ordered at  
127 level 1A and were orthorectified and registered using the algorithms of Baillarin et al, 2008. The  
128 absolute calibration of the sensor was obtained using the desert sites method (Cabot et al, 2000). 30  
129 to 50 images are available for both sites.

130 As FORMOSAT-2 lacks SWIR bands, it is not perfectly suited to simulate SENTINEL-2 time series  
131 and to test the enhancements brought by these bands. For this purpose, we use time series acquired  
132 between 1999 and 2003, combining LANDSAT 5 Thematic Mapper and LANDSAT 7 Enhanced  
133 Thematic Mapper data, when both instruments were fully operational (cf LANDSAT Handbook).  
134 We have used 3 data sets taken by both LANDSAT satellites during the whole year 2002, in the  
135 USA : Fresno, Boulder, Columbia (See table 2 for sites coordinates). These products are  
136 orthorectified and calibrated (L1T products). On average, each time series is made of about 35 non  
137 completely cloudy images.

### 138 **3. Multi Temporal Cloud Detection (MTCD) method**

139 Compared to MODIS and LANDSAT, VEN $\mu$ S and FORMOSAT-2 lack thermal infra-red and short  
140 wave infrared bands. VEN $\mu$ S and FORMOSAT-2 have spectral bands in the blue, but it is well  
141 known that the histograms for clouds and surface reflectances overlap to such an extent that thin  
142 clouds or bright land surfaces may often be confused (Bréon and Colzy 1999). For instance, figure 1  
143 shows the histogram overlap of blue reflectance, for a FORMOSAT-2 scene in Tensift, in a hard  
144 case (bright ground, thin clouds). On the same figure (bottom plot), one can note a better histogram  
145 separation for the reflectance difference between two successive acquisitions. In this figure, the  
146 cloud notation results from our method described below, but the validity of the cloud classification

147 has been checked by visual inspection, as it may be seen on figure 2.

148 As a result, our main criterion to detect clouds is a threshold on the reflectance increase in the blue  
149 spectral band. To compute the variations and detect clouds for the image of day D, a cloud free  
150 reference image is needed, and as it is not always available, it has to be build from partly cloudy  
151 images. Our clear image is a composite image that contains for each pixel the most recent cloud free  
152 reflectance obtained in the time series before date D. Our algorithm works at 100m resolution for  
153 FORMOSAT2 and 240m for LANDSAT, mainly for computing performance reasons, but also to  
154 avoid possible image registration errors. A pixel is flagged as cloudy for the multi temporal criterion  
155 if :

$$156 \quad [\rho_{\text{blue}}(D) - \rho_{\text{blue}}(D_r)] > 0.03 * (1 + (D - D_r) / 30) \quad (1)$$

157 where  $\rho_{\text{blue}}(D)$  is the pixel reflectance in the blue band, corrected for Rayleigh scattering,  
158 at date D, and  $D_r$  is the date of the most recent cloud free data before date D;  $D - D_r$  is expressed in  
159 days. The threshold value depends on the number of days between D and  $D_r$  . When dates are very  
160 close, the threshold tends to 0.03, but this value doubles when  $D_r$  and D are separated by 30 days,  
161 to allow a change in surface reflectances.

162 Although this criterion proves very efficient to separate cloudy and cloud free pixels above land  
163 surfaces, it is of course not foolproof. First, it does not work well above inland water surfaces,  
164 which are prone to sudden variations of reflectance because of sunglint, turbidity or foam. Water  
165 pixels must be discarded before computing the cloud mask. Second, thin clouds and high aerosol  
166 optical thicknesses may be confused : some clouds may be too thin to be detected (see Fig 4),  
167 whereas high variations of AOT may be regarded as clouds. Third, sudden variations of surface  
168 reflectances may occur, due to agricultural interventions (cropping, ploughing), or to natural  
169 variations such as fires or snow, or just to a quick drying of vegetation. To cope with these  
170 problems, two tests were added to check if a sudden reflectance increase is really due to a cloud. A  
171 pixel that verifies equation (1) is finally not flagged as cloudy if any of the 2 following conditions is  
172 true :

173 •i) If the variation of reflectance in the red band is much greater than the reflectance variation in the



174 blue : this happens quite often when a field is cropped or ploughed, or when vegetation dries  
175 quickly.

$$176 \quad \rho_{red}(D) - \rho_{red}(D_r) > 1.5 * (\rho_{blue}(D) - \rho_{blue}(D_r)) \quad (2)$$

177 where  $\rho_{red}(D)$  is the pixel TOA reflectance in the red band, corrected from  
178 Rayleigh scattering.

179 •ii) if the reflectances in the pixel neighborhood are well correlated with those of the same  
180 neighborhood in one of the ten images acquired before date D. Such a test was already used by  
181 Lyapustin et al, 2008 : as it is very unlikely that a cloud stays at the same place with a constant  
182 shape, a good correlation coefficient can only be due to a good transparency of the atmosphere.  
183 Using the ten previous images instead of the composite images enables to cope with a possible  
184 initial error in the composite. For instance, a case was found in which plastic greenhouses were  
185 installed on a field : the condition of equation (1) is met and the pixel is flagged as cloudy. Being  
186 cloudy, the pixel is not used to update the composite, and the subsequent days would still be  
187 flagged as cloudy because the condition of equation (1) would remain true. Since the correlation  
188 between two successive images with the greenhouse is high, the criterion ii) reclassifies the pixel as  
189 unclouded. Thanks to that, the greenhouse is only marked as a cloud on a single date, instead of a  
190 long duration. This scheme can also work with snow, provided the snow cover does not change  
191 much after the fall. This correlation test also enables to classify as unclouded the images with a high  
192 AOT, but it sometimes reclassifies as unclouded the images with very thin clouds. Finally, we found  
193 out that images with an AOT under 0.7 at 550 nm are classified as unclouded whereas images with  
194 an AOT above 1 are classified as mostly cloudy. But this assertion is based on a very limited  
195 number of images, because of the scarcity of high AOT images on our time series.

196 The MTCO method is a recurrent algorithm for which the images must be processed in  
197 chronological order ; as any recurrent process, our algorithm needs to be initialized. The first cloud  
198 mask of the first image in the time series is obtained by a simple threshold on the blue band  
199 reflectance, and the first composite image is thus the first image, without the cloudy pixels. In order  
200 to be conservative, the threshold is quite high so that bright surface reflectances are not classified as

201 cloudy. As a consequence, thin clouds are missed in this first cloud mask. To avoid a degraded  
202 quality for the first images of a time series, we have implemented a “backward processing” scheme.  
203 The first 6 to 10 images are processed in reverse chronological order, so that a correct cloud mask is  
204 obtained for the first image of the time series. Then, all the images of the time series are processed  
205 in chronological order, starting with a cloud mask of good quality.  
206 Finally, as LANDSAT and Sentinel-2 sensors include FORMOSAT spectral bands in their band  
207 setting, our algorithm is also fully applicable to LANDSAT and Sentinel 2, although with a  
208 somewhat reduced accuracy because of the reduced revisit frequency. We did not use LANDSAT  
209 TIR (Thermal Infrared) band because our algorithm is intended to be implemented for VEN $\mu$ S and  
210 SENTINEL-2, for which no TIR band is available. On the other hand, LANDSAT SWIR bands are  
211 used to separate snow and clouds, following the method of Irish, 2000. The snow test is based on  
212 the Normalized Difference Snow Index (NDSI), defined as :

$$213 : NDSI = \frac{\rho_{Green}(D) - \rho_{SWIR}(D)}{\rho_{Green}(D) + \rho_{SWIR}(D)}$$

214 where  $\rho_{Green}(D)$  (resp.  $\rho_{SWIR}(D)$ ) is the TOA reflectance in LANDSAT green channel  
215 (resp. LANDSAT SWIR channel at 1.6 $\mu$ m). Clouds and snow reflectances are high in the green  
216 band, but snow reflectance is much lower in the SWIR. As a result, a bright pixel is flagged as snow  
217 if  $NDSI > 0.6$ .

218 Finally, the cloud masks are dilated since it is very common to observe thin clouds at the edge of  
219 thicker clouds. Dilatation is 2-pixel wide at reduced resolution, ie 200m for FORMOSAT-2 and  
220 480m for LANDSAT.

## 221 **4. Algorithm assessment**

222 The validation of a cloud mask is a hard task. First, there is a continuity between haze and clouds,  
223 and defining a precise limit between them is subjective. Second, there is no reliable independent  
224 source of cloud mask at a given hour : all remote sensing cloud masks are imperfect, and ground  
225 truths, for instance using a ground based Lidar, only provide a very local information not suitable

226 for a comparison with a high resolution image. Bréon and Colzy (1999) have used synoptic  
227 observations from weather stations, but those only provide an average idea of the cloud cover in the  
228 vicinity of the station, which cannot be used to validate a high resolution cloud mask.

229 Lavanant et al, 2007 have used a data set of more than ten thousand low resolution vignettes  
230 classified by specialized photo interpreters to test their algorithms. Our algorithms have been  
231 applied to more than 300 FORMOSAT-2 images and more than 100 LANDSAT Images, and  
232 validated visually, but of course, it is not possible to show all these images here. For FORMOSAT-2  
233 satellite, Taiwan National Space Organization (NSPO) performs a cloud notation on all the images :  
234 an operator simply estimates visually the cloud cover percentage on each image. Figure 4 compares  
235 the cloud percentage from MTCD method to that of NSPO, for the Tensift and Muret sites. The  
236 agreement is surprisingly good given the rough estimate made by NSPO. Disagreements are only  
237 observed in a small number of cases : some of them are shown on fig 4, with the MTCD contour  
238 overlaid. On most cases, MTCD cloud notation seems more accurate.

239 We followed the same method to validate the MTCD masks obtained with LANDSAT. The  
240 independent notation is issued from the Automatic Cloud Cover Assessment (ACCA, Irish et al,  
241 2006), and thus is not a result of photo interpretation. The ACCA algorithm makes an intensive use  
242 of LANDSAT thermal infrared band. The method applied to LANDSAT 7 is a refined version  
243 compared to LANDSAT 5 ; an assessment of those algorithms is available in Hollingsworth et al,  
244 1996. The authors show that compared to photo interpretation, these algorithms slightly  
245 underestimate the cloud cover, which is consistent with the results obtained on figures 6, 7, 8 and 9.

246 Figure 6 shows a good agreement for the simple cases with very low or very high cloud covers, but  
247 the MTCD cloud cover is often greater than the cloud cover estimate from LANDSAT. Compared to  
248 MTCD, the ACCA algorithm seems to underestimate the cloud cover. Although there are some  
249 outliers, the agreement is generally better with LANDSAT 7 than with LANDSAT 5, which is  
250 consistent with the fact that LANDSAT 7 ACCA method is an enhancement compared to  
251 LANDSAT 5. Four case studies are shown on Figures 7,8, 9, and 10. Figures 7, 8 and 9, correspond  
252 to images for which the MTCD cloud cover is much greater than the ACCA one. On figures 7 and 8

253 the MTCD cloud mask seems quite accurate and the ACCA value is obviously underestimated. On  
254 figure 9, the result assessment is more subjective. The left part of the image is very likely covered  
255 by thin clouds, but the surface beneath is still visible. In such a case, our choice is to flag these  
256 pixels as cloudy: thanks to VEN $\mu$ S and SENTINEL-2 frequent repetitivity, it is likely that another  
257 cloud free image will be available just before or after this one.

258 In a very limited number of cases (one for each site), the ACCA provides a greater cloud cover than  
259 MTCD. These cases happen when some snow cover is present like in figure 10 right. Even if the  
260 cloud masks agree for simple cases like figure 10 left, some disagreements are observed in some  
261 complex cases such as figure 10 right where thin clouds are above snow. The MTCD cloud and  
262 snow detection seems accurate whereas the origin of the overestimation of the ACCA cloud mask is  
263 difficult to tell, as only the cloud percentage obtained by ACCA is available.

## 264 **5. Summary and Conclusions**

265 A Multi-Temporal Cloud Detection method (MTCD) has been developed in the framework of the  
266 preparation of VEN $\mu$ S and SENTINEL-2 Level 2 processors. The MTCD method makes a full use  
267 of VEN $\mu$ S and SENTINEL-2 capacity for producing time series of images, with a frequent revisit  
268 and under constant viewing angles. The algorithm is mainly based on a threshold on reflectance  
269 temporal variation in the blue band, but is complemented by a few criteria designed to avoid false  
270 detections : comparison of reflectance variations in the blue and in the red spectral bands, and a test  
271 of the local correlation between the image to classify and the previously acquired images.

272 The method has been tested on two types of satellites, FORMOSAT-2 and LANDSAT 5 & 7, using  
273 the same parameter set. The validation of this cloud mask was made by visual inspection and by  
274 comparison with the cloud notation performed for the FORMOSAT2 and LANDSAT data catalogs.  
275 For FORMOSAT-2, the results obtained with MTCD compare well with the visual notation  
276 performed manually by operators at NSPO. For most of the disagreeing cases, a visual inspection  
277 shows that MTCD is more accurate. Compared to the Automatic Cloud Cover Assessment (ACCA)  
278 from LANDSAT data catalog, the cloud cover assessed by MTCD is almost always greater than that

279 of ACCA method. In most of the studied cases, the MTCD is more accurate : this is a good  
280 performance, all the more so as the ACCA algorithm uses LANDSAT thermal infrared band, while  
281 we did not allow ourselves to use it because neither VEN $\mu$ S or SENTINEL-2 offer such a band.  
282 Some part of the differences between MTCD and ACCA masks are also related to our choice to  
283 provide the user with a very stringent cloud mask : the MTCD cloud mask is designed to be  
284 distributed with the product, and is also a preliminary step to perform accurate atmospheric  
285 corrections. This algorithm has been tuned to flag even very thin clouds, but even though, the  
286 amount of false detections remains low thanks to the good discrimination provided by the multi-  
287 temporal variation criteria.

288 However, the good discrimination capability of the MTCD algorithm has a drawback: for an  
289 operational ground segment, the MTCD method requires to process data in chronological order  
290 which limits the possibilities to process the images in parallel. Still, the MTCD method will be  
291 operationally used in VEN $\mu$ S ground segment for the production of level 2 products. Such a  
292 decision has not yet been taken for SENTINEL-2.

293 For the time being, we applied the MTCD method to the high resolution satellites that can produce  
294 time series with constant viewing angles (LANDSAT and FORMOSAT-2), but the availability of  
295 VEN $\mu$ S and SENTINEL-2 will give more opportunities for improvements : VEN $\mu$ S will offer a  
296 stereoscopic cloud mask thanks to two identical spectral bands with a viewing angle difference of  
297 about 1.5 degree, whereas SENTINEL-2 will bring a spectral band at 1.38  $\mu$ m which will enhance  
298 detection of high clouds.

## 299 **6.Acknowledgments**

300 This paper includes FORMOSAT-2 images which are material © NSPO (2005-2006), distribution  
301 Spot Image S.A. all rights reserved. We are grateful to CNES (DCT/ME/EI) for the geometrical  
302 processing of the FORMOSAT-2 images. We are also grateful to US Geological Survey for the free  
303 distribution of LANDSAT Images.

## 304 7. References

- 305 • S.A. Ackerman, K.I. Strabala, W.P. Menzel, R.A. Frey, C.C. Moeller, and L.E. Gumley (1998),  
306 “Discriminating clear sky from clouds with MODIS,” *Journal of Geophysical Research*, vol. 103, pp.  
307 32,141-32,157.
- 308 • S. Baillarin, P. Gigord, et O. Hagolle (2008), “Automatic Registration of Optical Images, a Stake for  
309 Future Missions: Application to Ortho-Rectification, Time Series and Mosaic Products,” *IEEE International  
310 Geoscience and Remote Sensing Symposium, 2008*. vol. 2 1112-1115
- 311 • F.M. Bréon et S. Colzy (1999), “Cloud detection from the spaceborne POLDER instrument and validation  
312 against surface synoptic observations,” *Journal of Applied Meteorology*, vol. 38, 777-785.
- 313 • F. Cabot, O. Hagolle, H. Cosnefroy, et X. Briottet (1998), “Inter-calibration using desertic sites as a  
314 reference target,” *IEEE International Geoscience and Remote Sensing Symposium Proceedings, 1998*.  
315 vol.5., 2713-2715
- 316 • G. Dedieu, A. Karnieli, O. Hagolle, H. Jeanjean, F. Cabot, P. Ferrier, et Y. Yaniv (2006), “Venus : A joint  
317 Israel-French Earth Observation scientific mission with High spatial and temporal resolution capabilities,”  
318 *Recent Advances in Quantitative Remote Sensing*, Valencia, Spain: J.A.Sobrino, 517-521.
- 319 • J. Dozier (1989), “Spectral signature of alpine snow cover from the Landsat Thematic Mapper,” *Remote  
320 Sensing of Environment*, vol. 28, 1989, 9–22.
- 321 • B.C. Gao (1993), A.F.H. Goetz, et W.J. Wiscombe, “Cirrus cloud detection from airborne imaging  
322 spectrometer data using the 1.38  $\mu\text{m}$  water vapor band,” *Geophysical Research Letters*, vol. 20, 1993, 301-  
323 304.
- 324 • J.I. Fisher, J.F. Mustard, and M.A. Vadeboncoeur (2006), “Green leaf phenology at Landsat resolution:  
325 scaling from the field to the satellite,” *Remote Sensing of Environment*, vol. 100, 2006, pp. 265-279.
- 326 • R. Irish (2000), “Landsat 7 automatic cloud cover assessment,” *SPIE proceedings series*, SPIE,  
327 vol. 4049, 348-355
- 328 • R.R. Irish, J.L. Barker, S.N. Goward, et T.J. Arvidson (2006), “Characterization of the Landsat-7 ETM  
329 Automated Cloud-Cover Assessment (ACCA) Algorithm,” *Photogrammetric Engineering & Remote  
330 Sensing*, vol. 72, 1179-1188
- 331 • O. Hagolle, G. Dedieu, B. Mougenot, V. Debaecker, B. Duchemin, et A. Meygret (2008), “Correction of  
332 aerosol effects on multi-temporal images acquired with constant viewing angles: Application to Formosat-2  
333 images,” *Remote Sensing of Environment*, vol. 112, 1689-1701.
- 334 • B. Hollingsworth, L. Chen, S.E. Reichenbach, et R. Irish (1996), “Automated cloud cover assessment for  
335 Landsat TM images,” *Proceedings of SPIE*, Vol. 2819, 170-179.
- 336 • L. Lavanant, P. Marguinaud, L. Harang, J. Lelay, S. Péré, et S. Philippe (2007), “Operational cloud  
337 masking for the OSI SAF global METOP/AVHRR SST product,” *EUMETSAT meteorological satellite  
338 conference*, 24-28.
- 339 • C. Latry, C. Panem, et P. Dejean (2007), “Cloud detection with SVM technique,” *IEEE International  
340 Geoscience and Remote Sensing Symposium, 2007*. 448-451.
- 341 • S. Le Hégarat-Masclé et C. André (2009), “Use of Markov Random Fields for automatic cloud/shadow  
342 detection on high resolution optical images,” *ISPRS Journal of Photogrammetry and Remote Sensing*, vol.  
343 64, 351-366.
- 344 • G. Lissens, P. Kempeneers, et F. Fierens (2000), “Development of a cloud, snow and cloud shadow mask  
345 for VEGETATION imagery,” *Proceedings of VEGETATION 2000 Symposium*, pp. 3-6.
- 346 • A. Lyapustin, Y. Wang, et R. Frey (2008), “An automatic cloud mask algorithm based on time series of  
347 MODIS measurements,” *Journal of Geophysical Research*, vol. 113, D16207.
- 348 • F. Maignan, F.M. Bréon, and R. Lacaze (2004), “Bidirectional reflectance of Earth targets: Evaluation of  
349 analytical models using a large set of spaceborne measurements with emphasis on the Hot Spot,” *Remote  
350 Sensing of Environment*, vol. 90 pp. 210-220.
- 351 • P. Martimor, O. Arino, M. Berger, R. Biasutti, B. Carnicero, U. Del Bello, V. Fernandez, F. Gascon, P.  
352 Silvestrin, et F. Spoto (2007), “Sentinel-2 optical high resolution mission for GMES operational services,”  
353 *IEEE International Geoscience and Remote Sensing Symposium*, 2677-2680.
- 354 • M. Reuter et J. Fischer (2004), “Identification of cloudy and clear sky areas in SEVIRI Images”  
355 *Geophysical Research Abstracts*, EGU 2004 Conference, Nice, 05270.

- 356 • R.W. Saunders et K.T. Kriebel (1988), “An improved method for detecting clear sky and cloudy radiances  
357 from AVHRR data,” *International Journal of Remote Sensing*, vol. 9, 123-150.
- 358 • B. Wang, A. Ono, K. Muramatsu, and N. Fujiwara (1999), “Automated detection and removal of clouds  
359 and their shadows from Landsat TM images,” *IEEE TRANSACTIONS on Information and Systems*, vol. 2,  
360 pp. 453-460.
- 361 • E.H. Wilson and S.A. Sader (2002), “Detection of forest harvest type using multiple dates of Landsat TM  
362 imagery,” *Remote Sensing of Environment*, vol. 80, pp. 385-396.
- 363 • <http://landsathandbook.gsfc.nasa.gov/handbook.html>, Landsat 7 science data users handbook,  
364 NASA.

*Table 1 Summary of the characteristics of sensors used in this study*

	VEN $\mu$ S	FORMOSAT-2	SENTINEL-2	LANDSAT 5+7
Multispectral Resolution	10 m	8 m	10-20-60 m	30 m
Repetitivity(days) with constant viewing angles	2	1	10 (1 satellite) 5 (2 satellites)	16 (1 satellite) 8 (2 satellites)
Field of view (km)	24	27	300	180
Spectral bands (approximate center, nm).	412, 443, 490, 560, 620, 667, 702, 742, 782, 865, 910	485, 566, 660, 819	443, 490, 560, 665, 705, 740, 775, 842, 865, 940, 1375, 1610, 2200	485, 565, 665, 820, 1650, 2190, 11400
Coverage	50 to 100 sites	a few sites	All lands	All lands
Launch date	2012	2004	2013 (Sentinel 2A), 2014 (Sentinel 2B)	1984 (Landsat 5) 1999 (Landsat 7)

*Table 2 Coordinates of the sites used in this article. The latitude and longitude of scene centre are provided, and for LANDSAT, the coordinates in World Reference System 2 (WRS-2) are provided.*

Site, Country	Satellite	Latitude-longitude	Path-Row coordinates (LANDSAT)
Muret, France	FORMOSAT	43.48, 1.18	
Tensift, Morocco	FORMOSAT	31.67,-7.60	
Boulder, USA	LANDSAT	40.25, -104.25	033 - 032
Columbia, USA	LANDSAT	34.45,-82.5	017 - 036
Fresno, USA	LANDSAT	36.15,-119.5	042 - 035



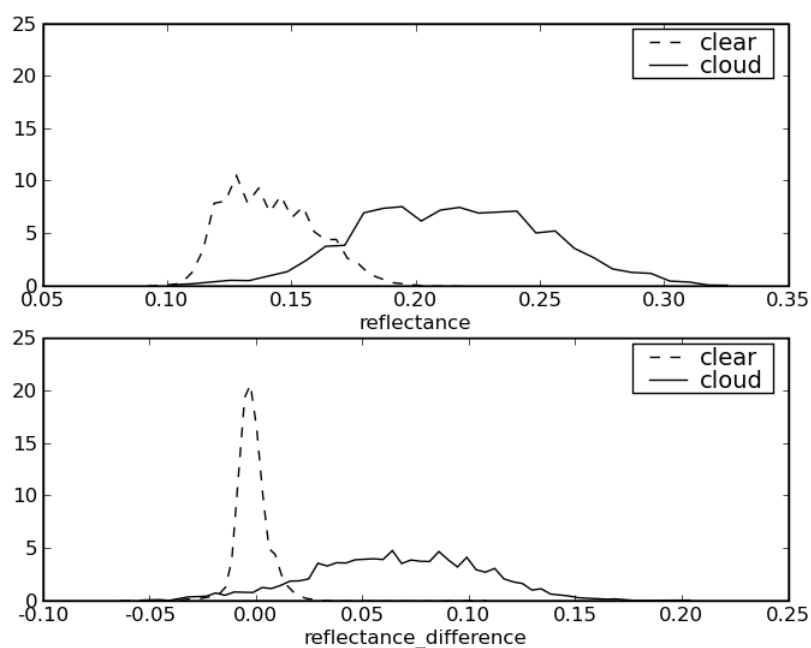


*Figure 1 : Comparison of histograms of clouded and unclouded pixels for FORMOSAT-2 blue band on Tensift site (Morocco), top : absolute reflectance on the April 13th, 2006, bottom: reflectance variation between the April 1<sup>st</sup> and the April 13th 2006. The image on April 1<sup>st</sup> is completely cloud free. Pixels within cloud shadows are not taken into account in the histograms.*

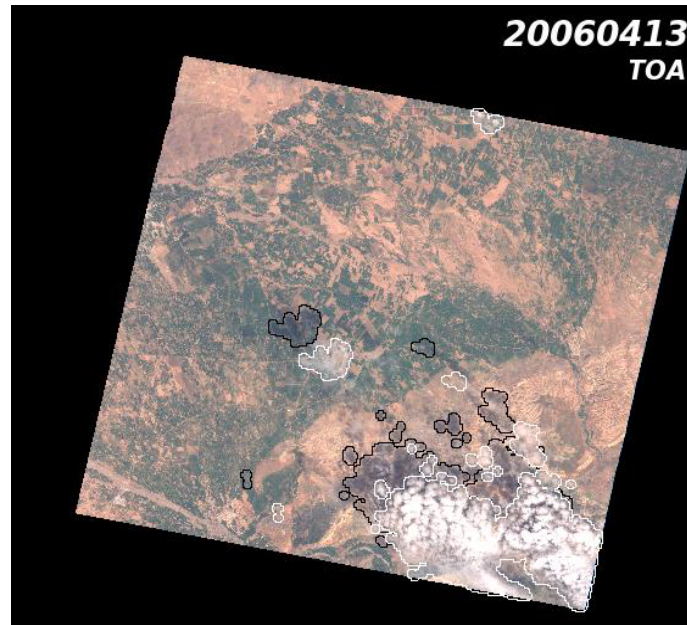


*Figure 2: color composite of FORMOSAT-2 red, green and blue Top of Atmosphere (TOA) reflectances for Tensift scene acquired on April 13th, 2006. Clouds detected by Multi Temporal Cloud Detection (MTCD) method are circled in white and cloud shadows are circled in black.*

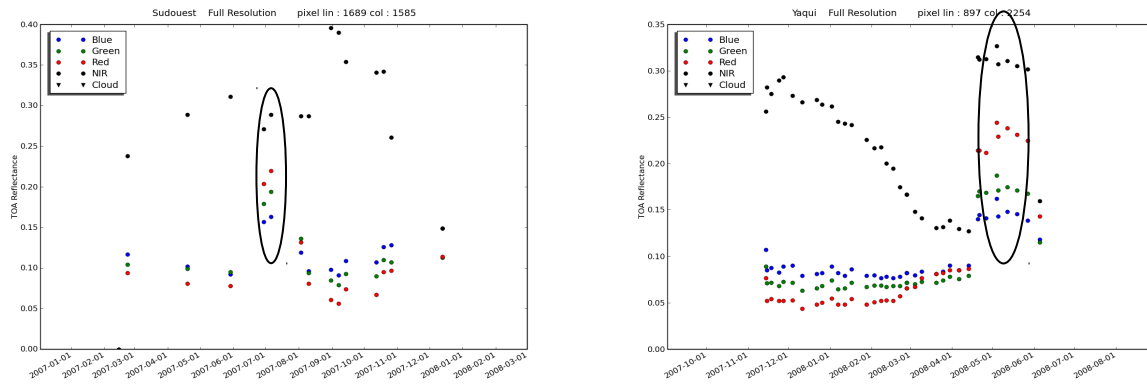


Figure 3: Temporal profile of cloud free TOA reflectances from FORMOSAT-2, left) for a pixel in a sorghum field near Muret (France), Right) for a wheat Field near Yaqui Mexico. On the left plot, the field is ploughed at the end of June, and before that date, was covered with sparse vegetation, on the right plot, the pixel is a wheat field which is cropped in may. For both sites and both dates, the test on the red variation corresponding to equation (2) prevents the circled pixels to be flagged as a cloud by the test on the Blue reflectance variation (equation 1).

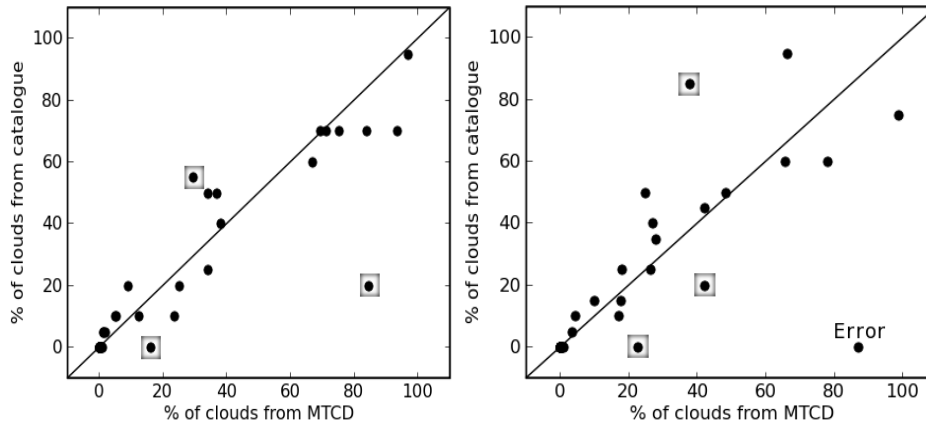
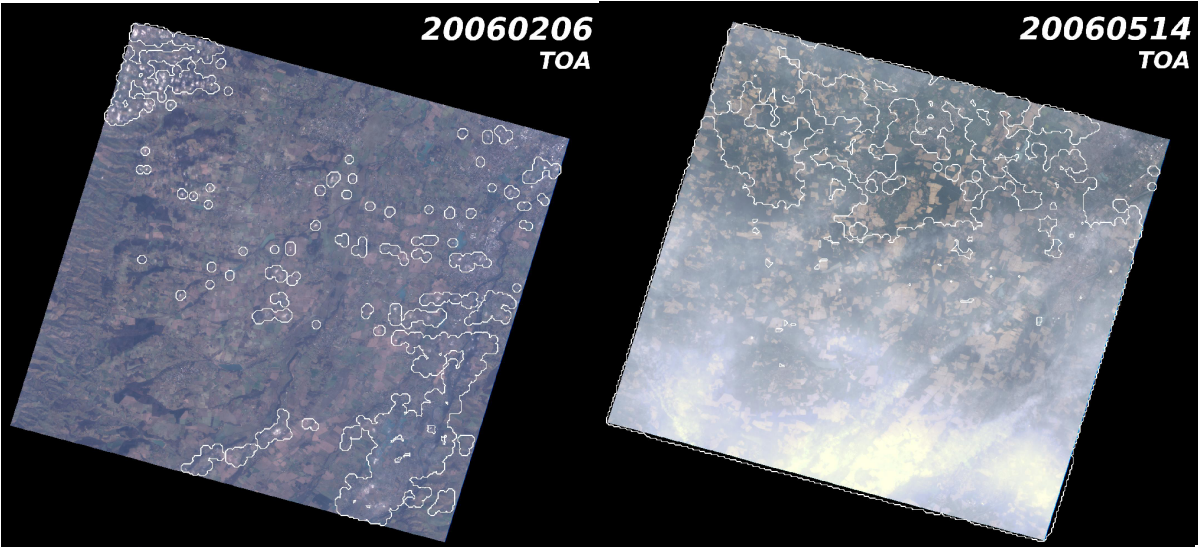
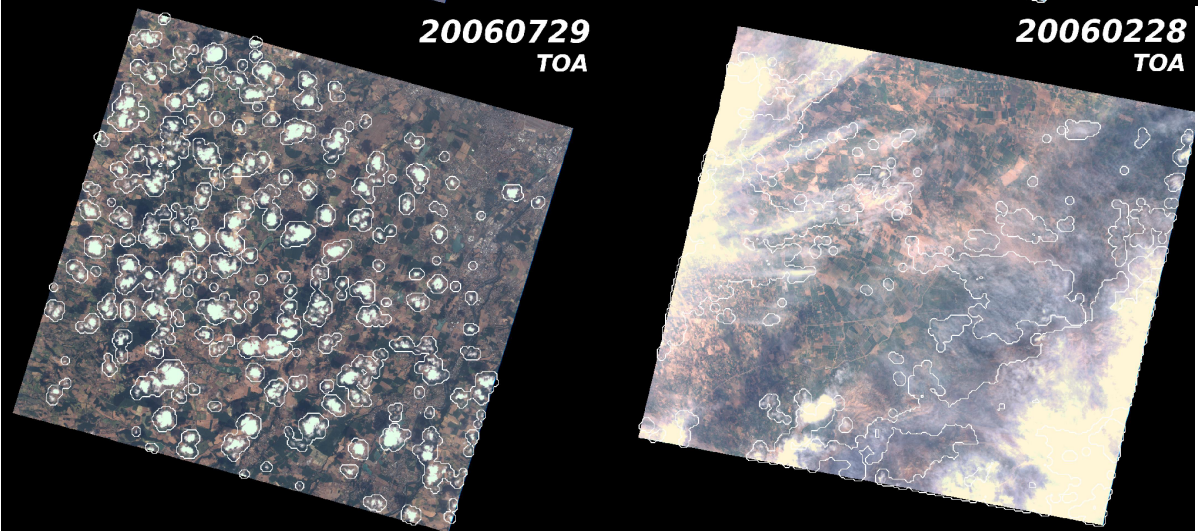


Figure 4 : comparison of the percentage of cloudy pixels on FORMOSAT-2 images estimated during NSPO manual cloud notation with the cloud percentage estimated by our multi-temporal method. Left, for Muret time series in France, Right for Tensift Time series. Large squares correspond to case studies shown on Figure 5, while the dot marked "error" corresponds to an obvious notation error from NSPO.

372



373



374

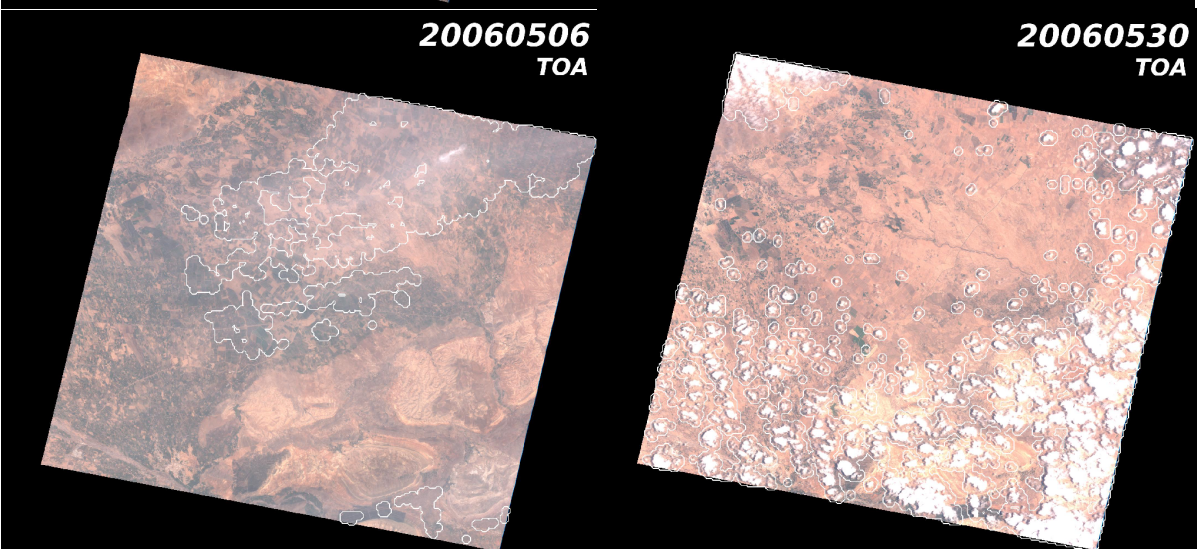
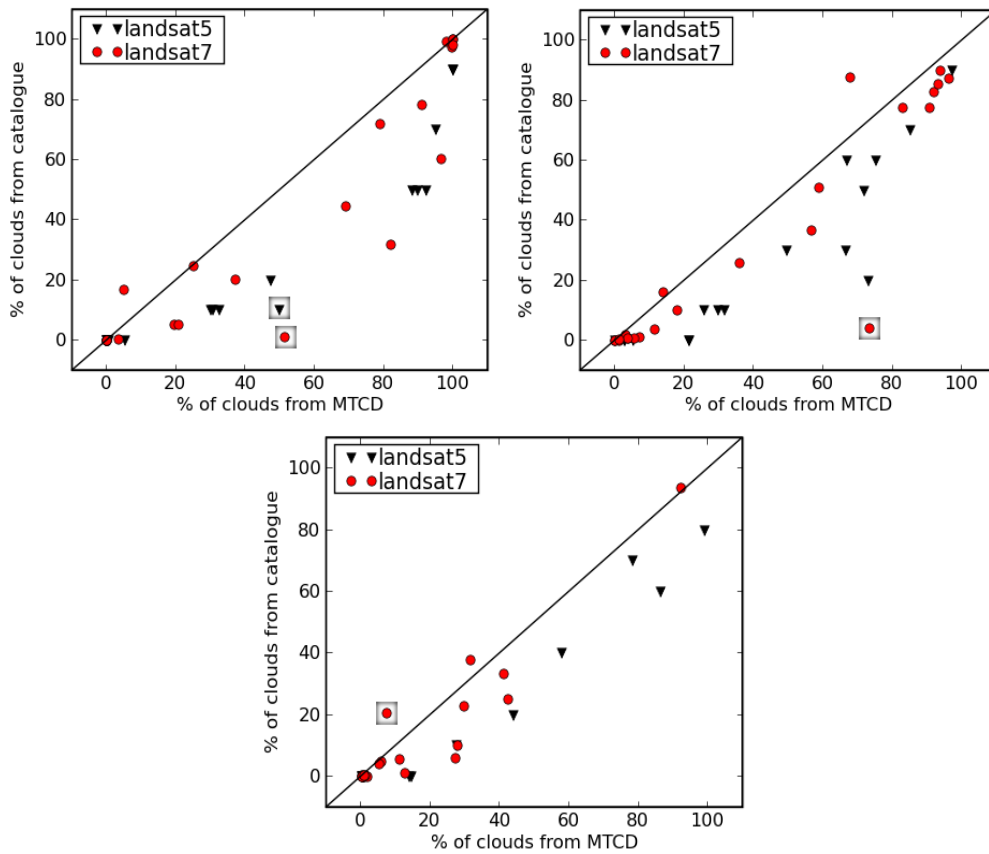


Figure 5 : visual verifications for a few cases identified in figure 3. White lines correspond to cloud contours from MTCD method. Upper Left) MTCD gives 12% of cloud cover, NSPO: 0%. Very small clouds can be seen, that were not seen by the operator. Upper Right) MTCD 80%, NSPO: 20%. Here, the operator probably only considered the thick clouds at the bottom of the image, but most of the image is evidently covered by thin clouds. Middle left) MTCD : 34%, NSPO 55%. The image is covered by small clouds, all of them seem to have been detected by MTCD. The operator has probably considered part of the space between clouds as cloudy. Middle right) MTCD 37%, NSPO 85%, the thin cloud cover is underestimated by our cloud mask because the previous image in the time series is quite old. Bottom Left) MTCD 22%, NSPO 0%. Thin clouds were not classified as clouds by NSPO operator. Bottom Right) MTCD 42%, NSPO 20%. The MTCD cloud cover looks accurate.

375



376

Figure 6 : Comparison of MTCD cloud cover percentage to LANDSAT ACCA algorithm from the LANDSAT catalog, left, on Columbia site (USA), right on Boulder site (USA), Bottom on Fresno site (USA) for all the images acquired in 2002. Circles correspond to LANDSAT 7, whereas triangles correspond to LANDSAT 5. Note that many points are in agreement when cloud percentage is close to 0 or 100. The large squares correspond to the images analyzed below (Figures 7 ,8, 9, and 10)

377

**20020507**  
**TOA**

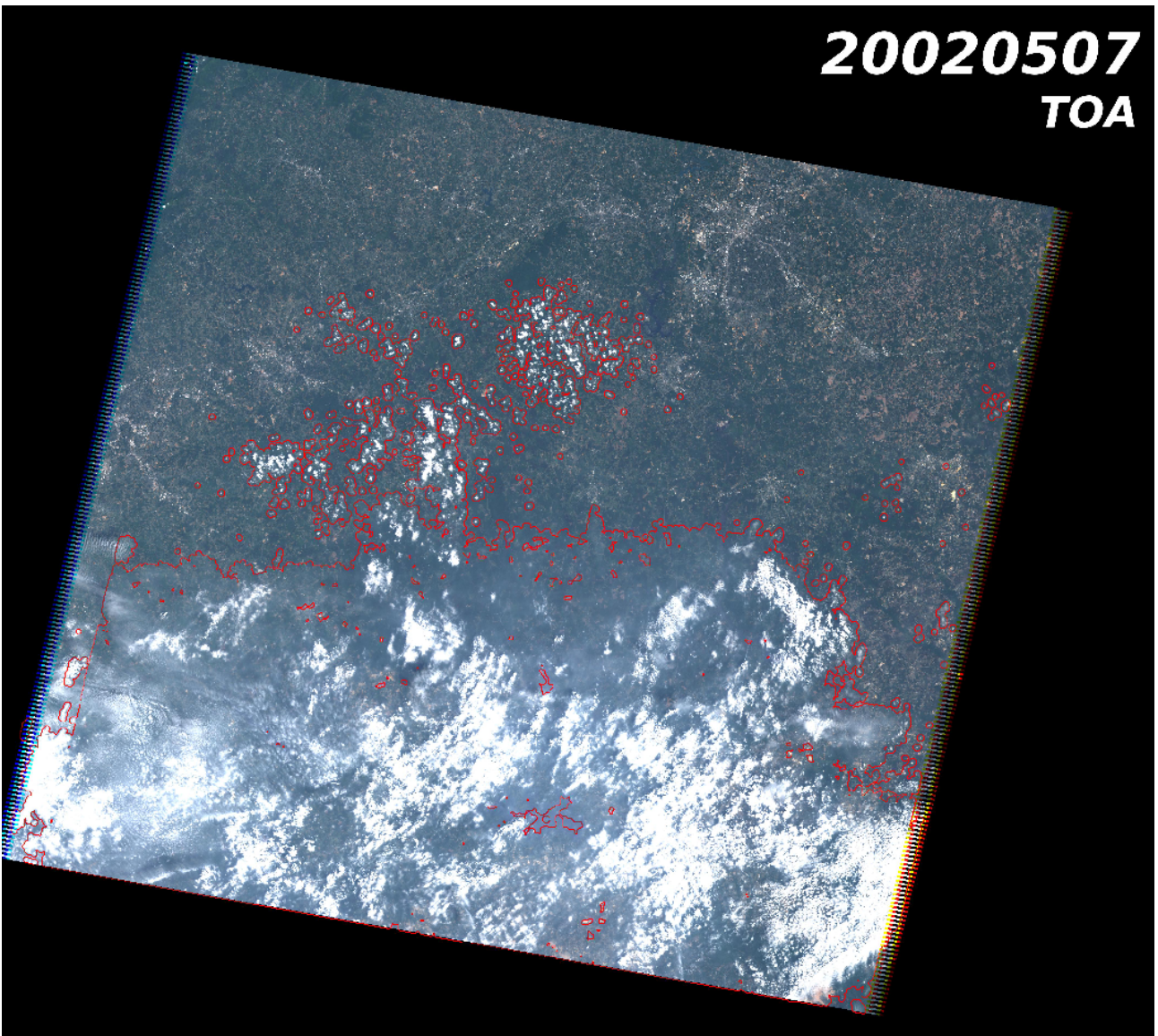


*Figure 7 :LANDSAT 5 image near Columbia, South Carolina, USA, for which cloud cover is 10% according to ACCA method and 49% according to MTCN method. Red lines correspond to MTCN image contours. The ACCA percentage is clearly underestimated.*

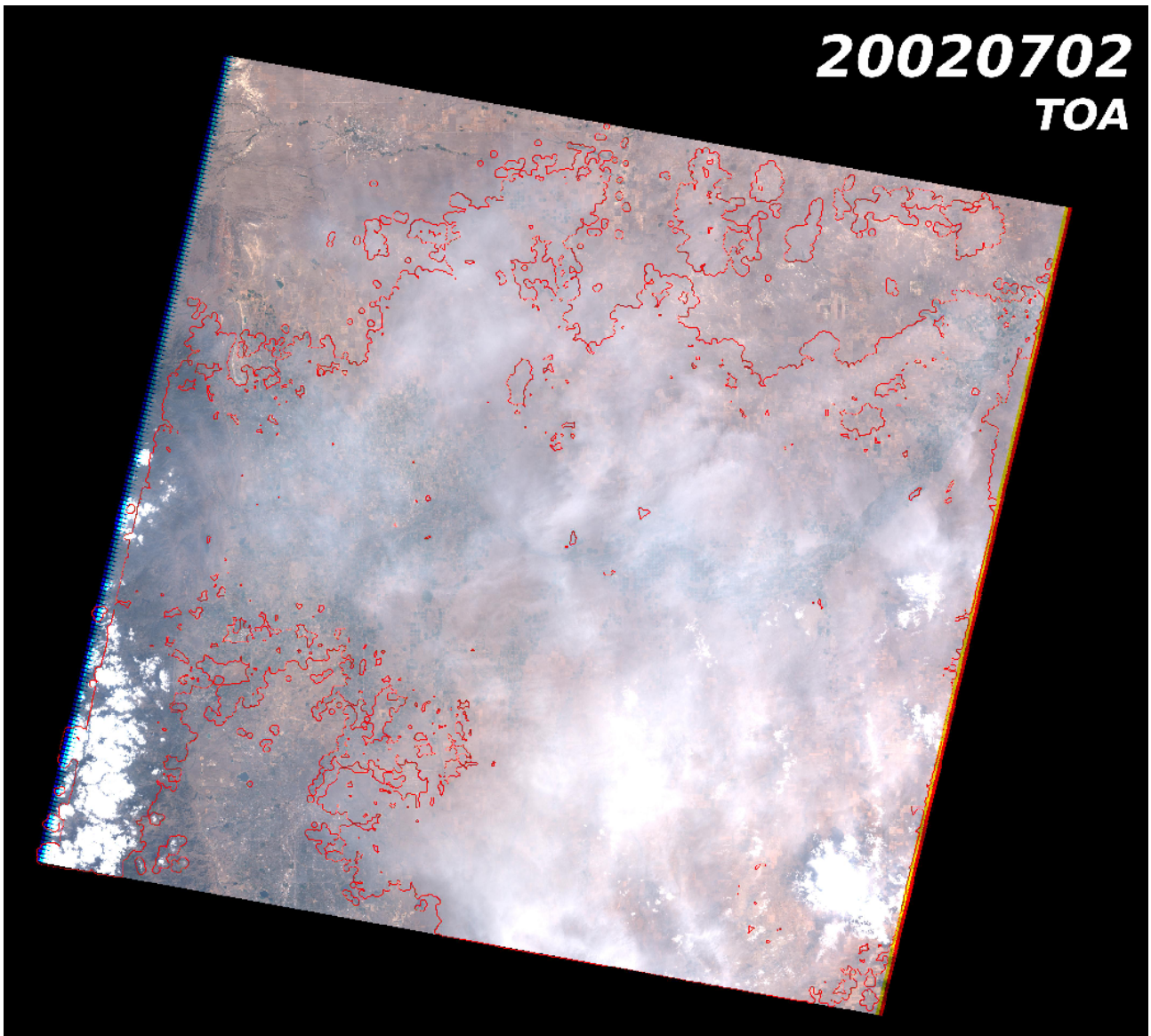
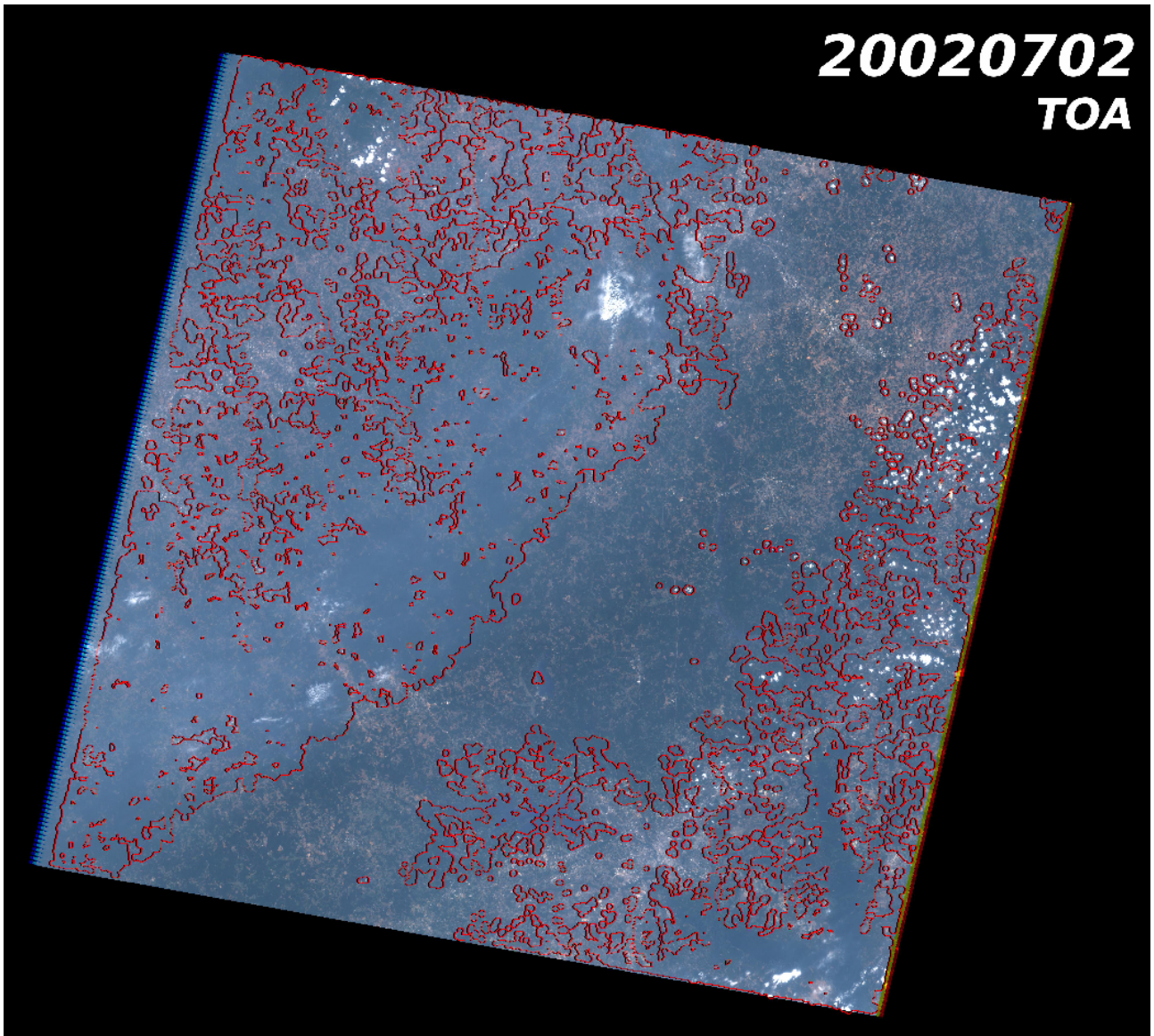


*Figure 8 :LANDSAT 7 image near Boulder USA, for which cloud cover is 4% according to data catalogue and 73% according to MTCD method. Red lines correspond to MTCD image contours. The ACCA percentage is clearly underestimated, and even the MTCD cloud mask misses some semi-transparent clouds in the upper left corner of the image.*

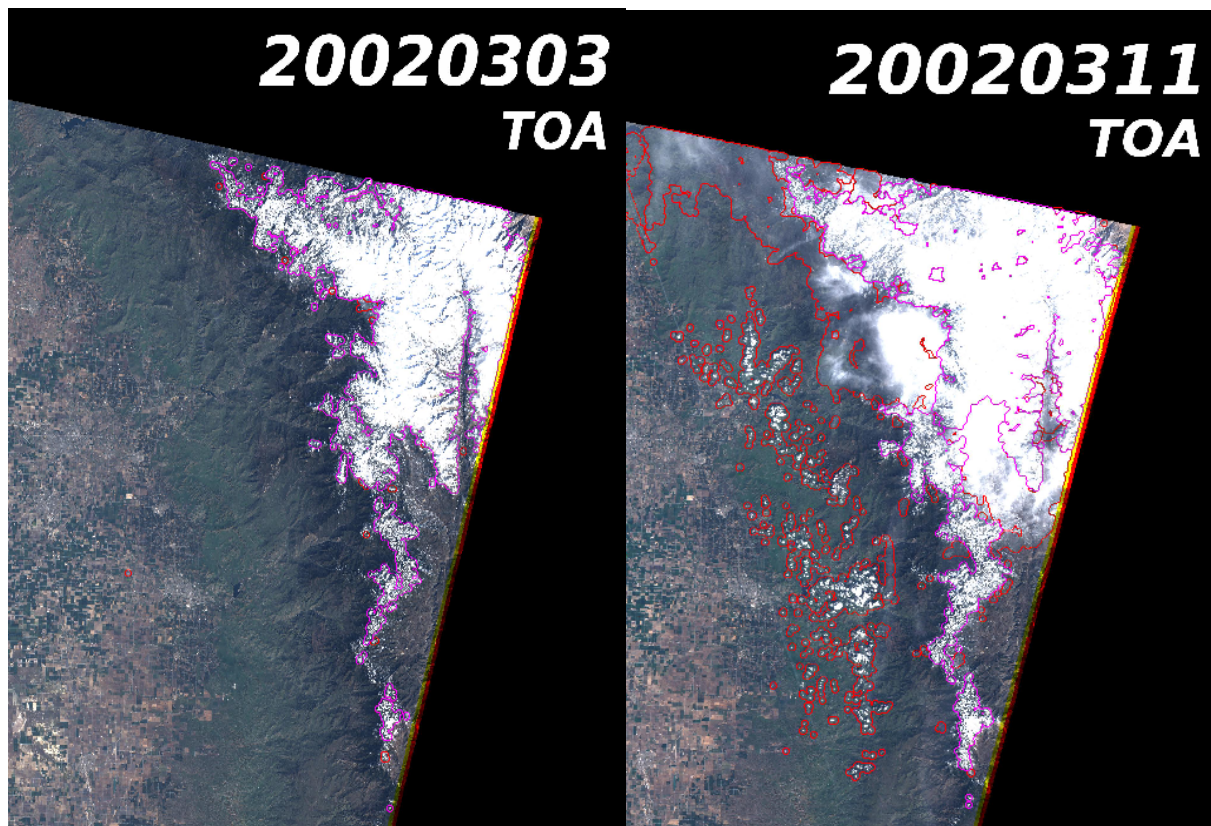




378

*Figure 9 :LANDSAT 7 image near Columbia, South Carolina, USA, for which cloud cover is 1.7% according to data catalogue and 51% according to MTC method. Red lines correspond to MTC image contours. Although the result of MTC method is maybe too strict, and its appreciation might be subjective, the ACCA percentage is clearly underestimated.*

379



380

*Figure 10 :LANDSAT 7 images extracts near Fresno California USA. Red lines correspond to MTCD image contours and pink lines to snow contours. On the image of the 3<sup>rd</sup> of March , ACCA and MTCD agree finding no cloud. For the image of the 11<sup>th</sup> of March, cloud cover is 20 % according to ACCA and 7% according to MTCD. The MTCD cloud and snow mask seems accurate, although it is a complex case with clouds above snow. MTCD probably finds more snow than ACCA.*